

# The structure of the electron outflow jet in collisionless magnetic reconnection

Michael Hesse, Seiji Zenitani, and Alex Klimas

Space Weather Laboratory, Code 674, NASA Goddard Space Flight Center,  
Greenbelt, Maryland 20771, USA

(Received 2 July 2008; accepted 2 October 2008; published online 10 November 2008)

Particle-in-cell simulations and analytic theory are applied to the study of the electron outflow jet in collisionless magnetic reconnection. In these jets, which have also been identified in spacecraft observations, electron flow speeds in thin layers exceed the  $E \times B$  drift, suggesting that electrons are unmagnetized. In this study, we find the surprising result that the electron flow jets can be explained by a combination of  $E \times B$  drifts and of diamagnetic effects through the combination of the gradients of particle pressure and of the magnetic field. In a suitably rotated coordinate system, the electron motion is readily decomposed into  $E \times B$  drift and the motion to support the required current density, consistent with electron gyrotopropy. This process appears to be nondissipative. © 2008 American Institute of Physics. [DOI: 10.1063/1.3006341]

## I. INTRODUCTION

Magnetic reconnection is arguably the most important transport process in collisionless plasmas. Magnetic reconnection facilitates large energy releases in solar plasmas,<sup>1</sup> magnetospheric plasmas,<sup>2</sup> and laboratory plasmas,<sup>3</sup> and it is believed to play a similarly important role in astrophysical plasmas as well.<sup>4</sup>

Owing to its importance, magnetic reconnection has attracted research based on space and laboratory probes, as well as based on theory and modeling. Recognizing the relevance magnetic reconnection has in space plasmas and for space weather, NASA has recently embarked on the Magnetospheric Multiscale mission, which will provide measurements on even the smallest relevant space and shortest time scales. In the meantime, addressing science questions currently inaccessible to direct measurements, the rapid progress of computational power has enabled theoretical research and modeling into the dynamics of the diffusion region, where the electric and magnetic fields and the electron flow velocity fulfill  $\vec{E} + \vec{v}_e \times \vec{B} \neq 0$ .

A combination of theory and numerical modeling has shown that the likely main contributor to the right hand side of this equation is provided by anisotropies in the thermal plasma inertia,<sup>5,6</sup> although there are indications that wave-particle interactions may be important in some cases.<sup>7</sup> The inertia-based process manifests itself in the nongyrotopropic pressure tensor, so that the third term of

$$\vec{E} + \vec{v}_e \times \vec{B} = -\frac{1}{en_e} \nabla \cdot \vec{P} - \frac{m_e}{e} \left( \frac{\partial \vec{v}_e}{\partial t} + \vec{v}_e \cdot \nabla \vec{v}_e \right) \quad (1)$$

is dominant in many if not most situations. Outside of this diffusion region we find first strong electron jets and, on larger scales, the ions jets commonly seen in spacecraft observations.

Recently, numerical modeling has revealed an interesting feature associated with the electron outflow jets. A set of numerical investigations by different groups revealed that the

electron jet velocity is faster than the drift speed provided by the local electric and magnetic fields, i.e., that the electrons appear to be decoupled from the magnetic field.<sup>8–10</sup> Observations show that this process appears to occur over very large distances from the diffusion region, of more than 60 ion inertial lengths.<sup>11</sup> The simulations found large variations in the electron pressure tensor in association with this electron jet, giving rise to the designation of an “outer diffusion region.”

In this paper, we will perform a detailed investigation of the physics of the electron outflow jet. We will utilize high-resolution, particle-in-cell simulations to analyze the local structure of the electron outflow jet.

## II. SIMULATION SETUP AND RESULTS

We employ dimensionless quantities. Densities are normalized by a typical density  $n_0$  in the current sheet and the magnetic field by the asymptotic value of the magnetic field  $B_0$ . Ions are assumed to be protons (mass  $m_p$ ) throughout, and length scales are normalized by the ion inertial length  $c/\omega_i$ , with the ion plasma frequency  $\omega_i = \sqrt{e^2 n_0 / \epsilon_0 m_p}$ . Velocity units are ion Alfvén velocity  $v_A = B_0 / \sqrt{\mu_0 m_p n_0}$  and the electric field is measured in units of  $E_0 = v_A B_0$ . Pressures and current densities are measured in units of  $p_0 = B_0^2 / \mu_0$  and  $j_0 = \omega_i B_0 / c \mu_0$ , respectively.

The initial condition consists of a modified Harris sheet and is of the form  $B_x = \tanh(2z)$ , with a superposed X-type initial perturbation. The system size is  $L_x = 102.4$  and  $L_z = 51.2$ . The ion-electron mass ratio is chosen to be  $m_i/m_e = 25$ . A total of  $3.2 \times 10^9$  macroparticles is moved on a singly periodic  $1600 \times 1600$  grid, with an electron/ion temperature ratio of  $T_e/T_i = 0.2$ .

Figure 1 shows a snapshot of the evolution at  $t = 80$ . The figure shows the poloidal ( $x$  and  $z$ ) components of the magnetic field and the  $x$  component of the electron flow velocity. The narrow electron flow channel extends for many ion inertial lengths from the X point, a feature noted before.<sup>8</sup> The

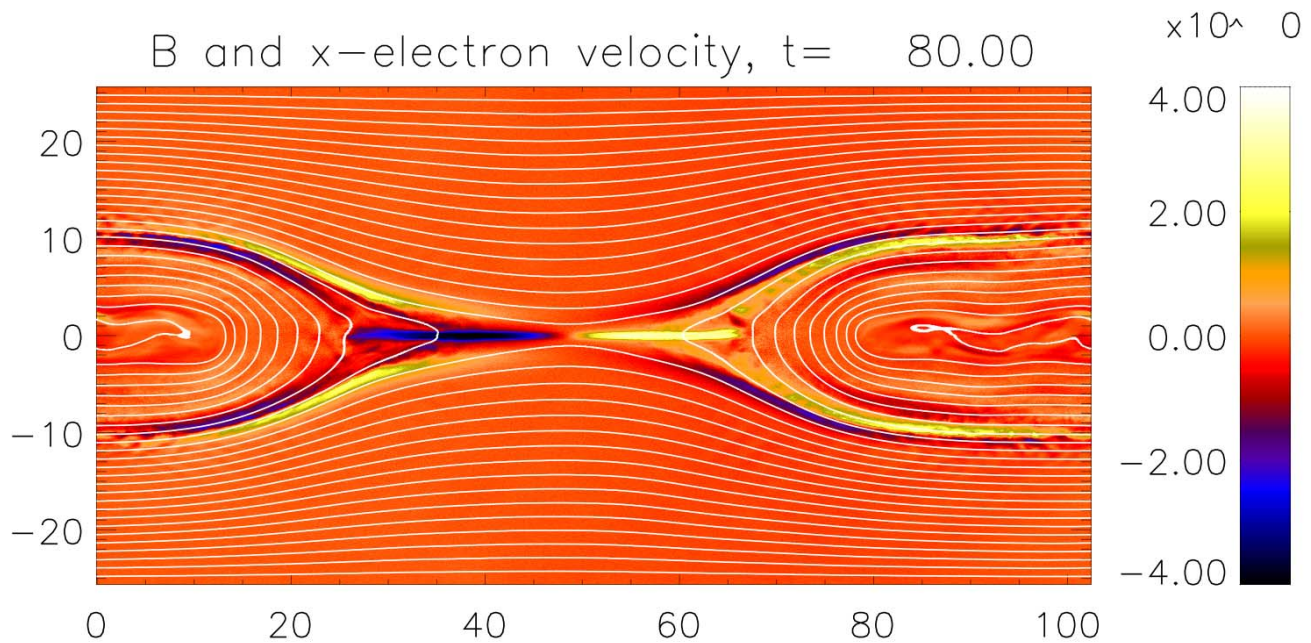


FIG. 1. (Color online) Magnetic field and  $x$  component of the electron flow velocity at  $t=80$ . The figure shows strong, extended, electron jets emanating from the diffusion region.

objective here is to understand the physics of this outflow jet.

The physical problem is illustrated in Fig. 2, which displays a cut in the  $z$  direction across the jet at  $x=55$ , where quantities near  $z=0$  are approximately invariant in  $x$ . Here, we find a substantially larger  $x$  component of the electron flow velocity than the velocity given by the  $x$  components of the  $\vec{E} \times \vec{B}$  drift speed. Along with these velocities, the figure also shows a large variation in the electron pressure tensor component  $P_{yze}$ , so that, in the vicinity of  $z=0$ ,

$$E_y - v_{ex}B = -\frac{1}{en_e} \frac{\partial P_{yze}}{\partial z}, \quad (2)$$

where the derivative of the electron pressure tensor component is large. It should be noted that the term on the right hand side of Eq. (2) is negative, i.e., has the opposite sign of the corresponding derivative in the electron diffusion region. Regardless of this, the apparent slippage between the electron flow and magnetic field gave rise to the term outer dissipation region.<sup>10</sup>

### III. ANALYSIS IN ROTATED FRAME

For an analysis of the underlying physics, it is helpful to consider the geometry of the system. For this purpose, Fig. 3 displays the variation in the magnetic field, as well as the  $x$  and  $y$  components of the electron number density flux  $nv$ . Apparently, near  $z=0$ , the  $y$  component of the magnetic field exceeds the  $x$  component, and both the  $x$  and  $y$  components are proportional to each other. This distortion is generated by the electron flow in the  $y$  direction. This proportionality suggests a new way to investigate the geometry of this process. We note that the strong variation in both components of the magnetic field implies that, locally, the magnetic field lies in

a plane tilted relative to the  $x$ - $z$  simulation plane.<sup>12</sup> This is schematically illustrated in Fig. 4, where the tangent plane to the magnetic field is spanned by the directions  $x'$  and  $y'$ .

The angle between the  $x$  axis and the plane spanned by the local magnetic field is approximately  $\alpha \approx 54^\circ$ . We point out that this angle is not generic but the result of this specific simulation. However, it is well known that the magnitude of

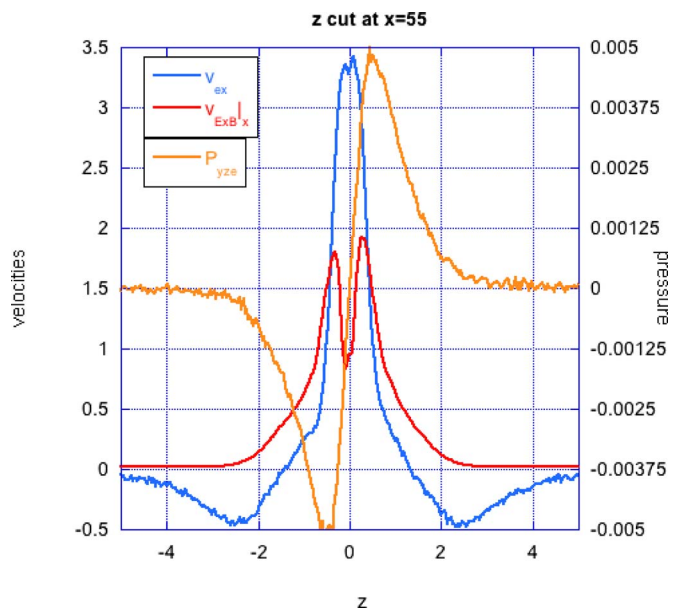


FIG. 2. (Color online) Cut in the  $z$  direction of the electron flow velocity, the  $x$  component of the electric field drift, and the electron pressure tensor component  $P_{yze}$ . The cut is taken at  $x=55$ . The figure shows a substantial deviation between the electron flow speed and the electric field drift, where the drift speed is roughly a factor of 3 smaller than the electron flow speed.

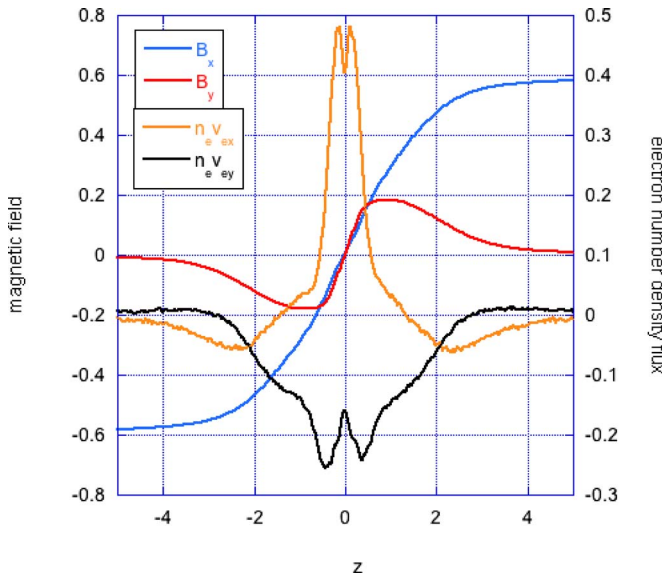


FIG. 3. (Color online) Similar to Fig. 2 but plots of the magnetic field variation and of the electron number density flux, i.e., the negative of the electron current densities.

the guide magnetic field is comparable to the antiparallel component in many simulations. Therefore, we expect angles of similar magnitude in most other simulations.

We will use this angle to calculate the physical quantities in the rotated coordinate system. For example, the magnetic field transforms like

$$\begin{aligned} B_{x'} &= B_x \cos(\alpha) + B_y \sin(\alpha), \\ B_{y'} &= -B_x \sin(\alpha) + B_y \cos(\alpha), \\ B_{z'} &= B_z. \end{aligned} \tag{3}$$

The transformed magnetic field and electron flow velocities are shown in Fig. 5. As is apparent from the figure, the transformed magnetic field component  $B_{y'}$  vanishes near  $z=0$ .

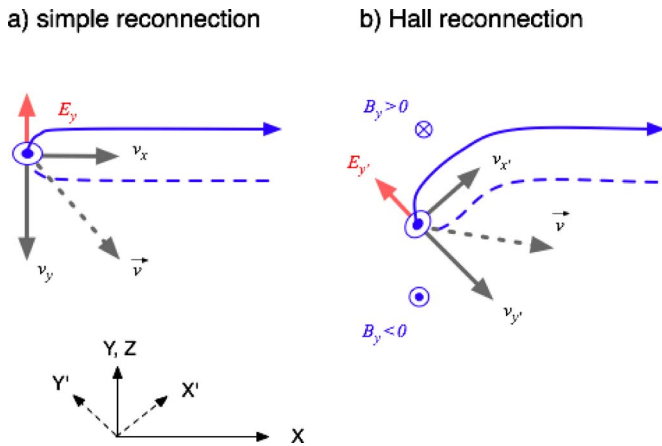


FIG. 4. (Color online) The figure illustrates the magnetic geometry of the outflow jet. The strong variation in both  $B_x$  and  $B_z$  implies a locally oblique tangent plane to the magnetic flux tube. The linear relation between the two magnetic field components renders this tangent plane well defined close to  $z=0$ . The main current flow is locally normal to the tangent plane.

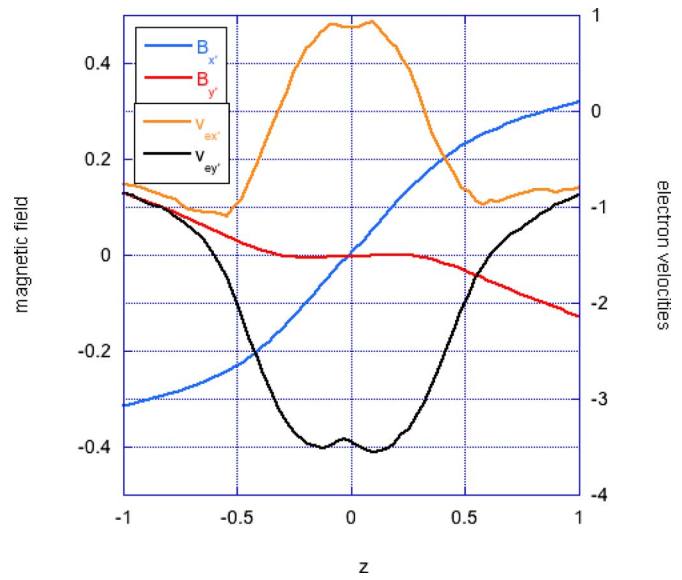


FIG. 5. (Color online) Magnetic fields and electron flow velocities in the rotated coordinate system. It is noteworthy that the  $y'$  component vanishes (by design) near  $z=0$ , and that the electron flow velocity in the  $x'$  direction is only of the order of the Alfvén velocity.

$z=0$ . This implies that, locally and near  $z=0$ , the quadrupolar magnetic field does not appear in this frame. However, moving further away from  $z=0$  shows evidence of the existence of the quadrupole.

The transformed electron flow velocity is primarily in the  $y'$  direction, consistent with the main current direction associated with the magnetic field reversal in the new coordinate system. A comparison between the electric field component  $E_{y'}$  and the electron convection electric field  $E_{cy'} = -v_{ez}B_{x'} + v_{ex'}B_z$  is shown in Fig. 6. We find a surprising

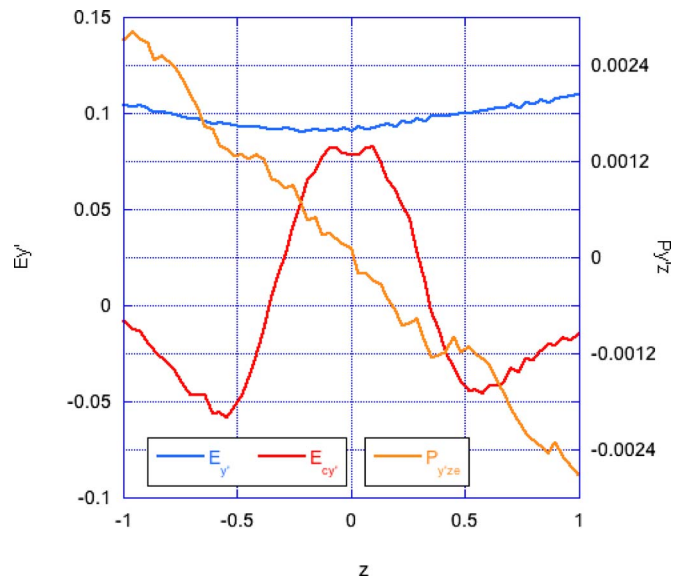


FIG. 6. (Color online) Electric field, convection electric field, and pressure tensor in the rotated coordinate frame. The figure demonstrates that the electric field is nearly matched by the convection electric field in the center of the flow channel. The derivative of the pressure tensor  $y'z$  component is now negative, and it accounts for the difference between the total and convection electric fields in the center of the jet.

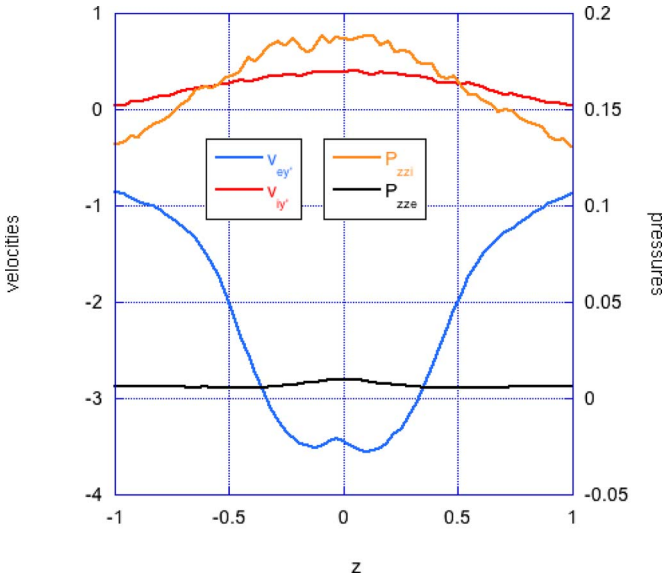


FIG. 7. (Color online) Electron and ion flow velocities in the  $y'$  direction, as well as the  $zz$  components of ion and electron pressure tensors.

match between the total and convection electric fields, with  $E_{y'} \sim 0.9$  and  $E_{cy'} \sim 0.8$ , indicating that the electrons are nearly completely frozen into the magnetic field in this frame. What is the source of the differences between  $E_{y'}$  and  $E_{cy'}$ ? Neglecting electron bulk inertia, these quantities are related by

$$E_{y'} = E_{cy'} - \frac{1}{en_e} \left( \frac{\partial P_{y'ze}}{\partial z} + \frac{\partial P_{y'y'e}}{\partial y'} \right). \quad (4)$$

It follows from translational invariance in  $y$  and approximate translational invariance in  $x$  that the second derivative vanishes near  $z=0$ , so that the small difference between the

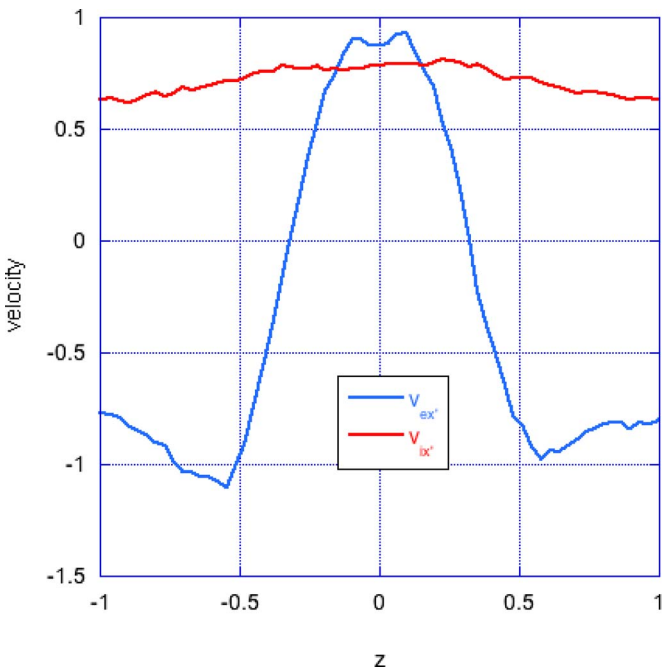


FIG. 8. (Color online) Electron and ion flow velocities in the  $x'$  direction.

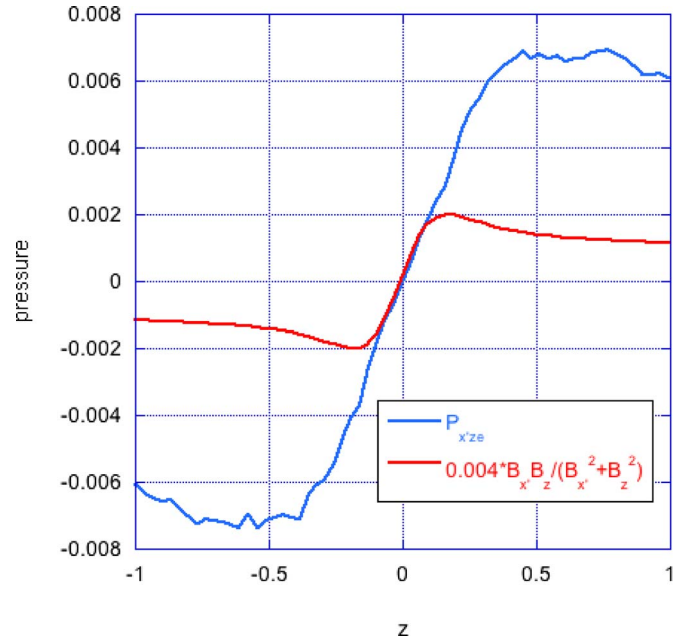


FIG. 9. (Color online) Pressure tensor component  $P_{x'ze}$  and approximation. The figure shows that the pressure is, to an excellent approximation, gyro-tropic in the current layer.

two quantities there is accounted for by the derivative of the pressure tensor component shown in Fig. 6. The second derivative plays a role at larger values of  $z$ , where the magnetic field is not planar anymore and where the approximate translational invariance in  $x$  is violated.

In the poloidal plane of the transformed coordinate system, the electron motion is determined by the  $E \times B$  drift. In this sense, the electrons are frozen into the magnetic field. The reason for the large velocities in the simulation frame is that the electrons provide most of the current associated with the magnetic field reversal of both  $B_x$  and  $B_y$ . In the transformed coordinate system, this is particularly easy to analyze. We find for the electron flow velocity in the  $y'$  direction

$$E_z + v_{ex'} B_{y'} - v_{ey'} B_{x'} = - \frac{1}{en_e} \left( \frac{\partial P_{x'ze}}{\partial x'} + \frac{\partial P_{y'ze}}{\partial y'} + \frac{\partial P_{zze}}{\partial z} \right). \quad (5)$$

Near our region of interest,  $B_{y'}$  as well as the last two terms in Eq. (5) vanish. Therefore, the electron flow velocity is determined by

$$v_{ey'} B_{x'} = E_z + \frac{1}{en_e} \frac{\partial P_{zze}}{\partial z}. \quad (6)$$

Similar arguments can be made for the ion flow velocity. Therefore, we get

$$v_{iy'} B_{x'} = E_z - \frac{1}{en_i} \frac{\partial P_{zzi}}{\partial z}. \quad (7)$$

Consistent with the small ion velocity shown in Fig. 7, the right hand side of Eq. (7) vanishes to within 10% of the peak value of  $E_z$ . Subtracting these two equations from each other, utilizing that the absolute magnitude of the electron

velocity is considerably larger than that of the ion velocity (Fig. 7), and assuming quasineutrality, we find

$$v_{ey'}B_{x'} \approx \frac{1}{en} \left( \frac{\partial P_{zzi}}{\partial z} + \frac{\partial P_{zze}}{\partial z} \right). \quad (8)$$

The first term on the right dominates due to the larger ion temperature. Equation (8) is the standard equation for a diamagnetic current sheet, where electrons carry the majority of the current due to momentum conservation.<sup>13</sup> The electron motion is thus a composite of  $E \times B$  drift and this current carrying velocity. This result is consistent with a nondissipative current sheet.

At this point, it is necessary to comment on the use of the term “dissipative.” Strictly speaking, dissipative refers to irreversible energy conversion, which, for example, in magnetohydrodynamics is related to resistive heating terms. In a kinetic plasma, the notion of dissipation is considerably more complex. At the reconnection site, dissipation is likely related to complex phase space structuring associated with strong initial condition dependence of particle orbits. The dissipation is then associated with phase mixing once the phase space has gotten sufficiently filamented. However, precise definition and description are still missing and should be the subject of future investigations. The outflow jet, on the other hand, appears to be a regular structure, which is readily explained by effects not commonly associated with dissipation, such as diamagnetic and  $E \times B$  drifts. It is in this sense that we use the term “nondissipative.”

Another interesting aspect is revealed when comparing the electron and ion velocities in the  $x'$  direction. The lack of a  $z$  gradient of  $B_{y'}$  implies that these velocities are essentially the same. This feature is evidenced by Fig. 8, and it implies that ions and electron outflows couple together at relatively small distances from the reconnection diffusion region when viewed in the proper frame.

Finally, Fig. 9 shows a graph of the pressure tensor component  $P_{x'ze}$  together with a fit to a function of the form  $P_{x'ze} = aB_z B_{x'} / B_{x'}^2 + B_z^2$ . The excellent fit between the two graphs proves that the electron pressure is essentially gyro-tropic in the electron flow channels, and that this gyrotropic

pressure balances the  $x'$  component of the Lorentz force<sup>14</sup> in a rotational discontinuity. We acknowledge that this fit appears to fail further away from  $z=0$ . This is due to two reasons: first, the neglect of  $B_{y'}$  is no longer justified there, and, second, further away from  $z=0$  we can no longer assume that the factor  $a$  above is independent of which field line is being considered.

In summary, we find that the very large electron outflow jet speeds in the simulation frame are explained by diamagnetic effects. In a suitably rotated coordinate system, the electrons carry most of the total current. Ions and electrons move at approximately the same velocity in the plane spanned by the magnetic field. This current sheet appears not to involve significant dissipation.

## ACKNOWLEDGMENTS

This research was supported by NASA’s MMS mission. One of us (S.Z.) gratefully acknowledges support from NASA’s postdoctoral program. The authors acknowledge helpful comments from Karl Schindler.

<sup>1</sup>H. E. Petschek, in *AAS/NASA Symposium on the Physics of Solar Flares*, edited by W. N. Ness (NASA, Washington, DC, 1964), p. 425.

<sup>2</sup>V. M. Vasyliunas, *Rev. Geophys. Space Phys.* **13**, 303, DOI: 10.1029/RG013i001p00303 (1975).

<sup>3</sup>M. Yamada, *Phys. Plasmas* **14**, 058102 (2007).

<sup>4</sup>S. Zenitani and M. Hoshino, *Phys. Rev. Lett.* **95**, 095001 (2005).

<sup>5</sup>M. Hesse, K. Schindler, J. Birn, and M. Kuznetsova, *Phys. Plasmas* **6**, 1781 (1999).

<sup>6</sup>K. Fujimoto, *Phys. Plasmas* **13**, 072904 (2006).

<sup>7</sup>J. F. Drake, M. Swisdak, C. Cattell, M. A. Shay, B. N. Rogers, and Z. Zeiler, *Science* **299**, 873 (2003).

<sup>8</sup>W. Daughton, J. Scudder, and H. Karimabadi, *Phys. Plasmas* **13**, 072101 (2006).

<sup>9</sup>H. Karimabadi, W. Daughton, and J. Scudder, *Geophys. Res. Lett.* **34**, L13104, DOI: 10.1029/2007GL030306 (2007).

<sup>10</sup>M. A. Shay, J. F. Drake, and M. Swisdak, *Phys. Rev. Lett.* **99**, 155002 (2007).

<sup>11</sup>T. D. Phan, J. F. Drake, M. A. Shay, F. S. Mozer, and J. P. Eastwood, *Phys. Rev. Lett.* **99**, 255002 (2007).

<sup>12</sup>M. E. Mandt, R. E. Denton, and J. F. Drake, *Geophys. Res. Lett.* **21**, 73, DOI: 10.1029/93GL03382 (1994).

<sup>13</sup>K. Schindler and M. Hesse, *Phys. Plasmas* **15**, 042902 (2008).

<sup>14</sup>F. A. Rich, V. M. Vasyliunas, and R. A. Wolf, *J. Geophys. Res.* **77**, 4670, DOI: 10.1029/JA077i025p04670 (1972).